Efflorescence upon humidification? X-ray microspectroscopic in situ observation of changes in aerosol microstructure and phase state upon hydration

Christopher Pöhlker[1], Jorge Saturno[1], Mira L. Krüger[1], Jan-David Förster[1], Markus Weigand[2], Kenia T. Wiedemann[3,4,5], Michael Bechtel[2], Paulo Artaxo[3], and Meinrat O. Andreae[1]

[1]Biogeochemistry and Multiphase Chemistry Departments, Max Planck Institute for Chemistry, Mainz, Germany, [2]Max Planck Institute for Intelligent Systems, Stuttgart, Germany, [3]Institute of Physics, University of São Paulo, São Paulo, Brazil, [4]School of Engineering and Applied Sciences, Harvard University, Cambridge, Massachusetts, USA, [5]Ecology and Evolutionary Biology Department, University of Arizona, Tucson, Arizona, USA

Abstract The phase and mixing state of atmospheric aerosols is a central determinant of their properties and thus their role in atmospheric cycling and climate. Particularly, the hygroscopic response of aerosol particles to relative humidity (RH) variation is a key aspect of their atmospheric life cycle and impacts. Here we applied X-ray microspectroscopy under variable RH conditions to internally mixed aerosol particles from the Amazonian rain forest collected during periods with anthropogenic pollution. Upon hydration, we observed substantial and reproducible changes in particle microstructure, which appear as mainly driven by efflorescence and recrystallization of sulfate salts. Multiple solid and liquid phases were found to coexist, especially in intermediate humidity regimes. We show that X-ray microspectroscopy under variable RH is a valuable technique to analyze the hygroscopic response of individual ambient aerosol particles. Our initial results underline that RH changes can trigger strong particle restructuring, in agreement with previous studies on artificial aerosols.

1. Introduction

Atmospheric aerosols play a crucial role in the climate system and hydrological cycle by scattering and absorbing sunlight and affecting the formation and development of clouds and precipitation [*Rosenfeld et al.*, 2008; *Solomon et al.*, 2007]. Their scattering and absorption properties as well as their ability to act as cloud condensation nuclei and ice nuclei depend on aerosol particle composition, size, morphology, mixing, and phase state [*Andreae and Rosenfeld*, 2008; *Jacobson*, 2001; *Ramanathan et al.*, 2001]. Mixing and phase effects in aerosol particles have substantial impacts on the particles' physical and chemical properties [*Koop et al.*, 2011; *Krieger et al.*, 2012; *Wang et al.*, 2008].

The phase state of aerosol particles strongly depends on their water content and, therefore, on changes in ambient relative humidity (RH) [*Mikhailov et al.*, 2009]. It can provoke substantial transformations of the aerosol properties [*Koop et al.*, 2011; *Martin*, 2000; *Shiraiwa et al.*, 2013; *Wang et al.*, 2008]. The dynamic response of aerosols to fluctuations in atmospheric conditions (i.e., RH and temperature) complicates an assessment of aerosol properties and impacts. The hygroscopic properties of aerosol components are commonly characterized by their deliquescence (liquefaction of solid particle) and efflorescence (solidification of supersaturated solution) relative humidities (DRH and ERH), as well as their RH-dependent hygroscopic growth. Pure inorganic particles, such as sodium chloride (NaCl) and sodium bromide (NaBr), often occur in (poly)crystalline states and undergo a hydration and dehydration cycle that is characterized by prompt phase transitions at DRH and ERH. In contrast, the most abundant submicrometer aerosol types in the atmosphere comprise amorphous, multicomponent, and internally mixed particles with inorganic salts, carbonaceous compounds, and water as their main constituents [e.g., *Lee et al.*, 2002; *Posfai et al.*, 1999]. Such particles exhibit a more diverse hygroscopic behavior, which can be characterized by gradual deliquescence and efflorescence, involving semisolid (e.g., rubber- or gel-like) intermediate states [*Mikhailov et al.*, 2009; *Shiraiwa et al.*, 2013].

Many studies have addressed the hygroscopic properties of aerosol particles with a variety of different techniques, such as hygroscopic tandem differential mobility analysis, microscopy, spectroscopy, and elastic light scattering [e.g., *Mikhailov et al.*, 2009; *ten Brink et al.*, 2000; *Wise et al.*, 2005]. Among them, microscopy is

used as a valuable tool to monitor morphological and phase changes in individual aerosol particles upon hydration and dehydration [*Peckhaus et al.*, 2012; *Song et al.*, 2012; *You et al.*, 2012]. However, these techniques have almost exclusively been applied to laboratory-generated particles, with the exception of a few studies on ambient particles by environmental electron microscopy [*Adachi et al.*, 2011; *Ebert et al.*, 2002; *Freney et al.*, 2010]. Scanning transmission X-ray microscopy with near-edge X-ray absorption fine structure analysis (STXM-NEXAFS) has become a well-established technique in aerosol science and has contributed important insights into aerosol microstructure and composition on a nanometer scale [e.g., *Moffet et al.*, 2012; *Russell et al.*, 2002; *Tivanski et al.*, 2007]. It combines microscopic imaging of the particles with chemical sensitivity to a variety of elements and functional groups. However, an uncertainty of this and many other sampling-based techniques is the alteration of the particles' morphology and composition (i.e., water content) as a consequence of drying during sampling, storage, and offline analysis. Therefore, the physical and chemical appearance of aerosol particles in postsampling analysis is expected to differ substantially from their constitution under ambient atmospheric conditions (supporting information, section S1). Recent studies have started to address this uncertainty by combining STXM analysis with the ability to observe laboratory-produced aerosol particles over a wide range of RH levels [*Ghorai and Tivanski*, 2010; *Zelenay et al.*, 2011].

In this study, we present an investigation using X-ray microspectroscopy on ambient submicrometer aerosols under variable RH conditions, showing in situ changes in morphology, microstructure, and phase state upon humidity cycling. The analyzed aerosol samples were collected in the Amazonian rain forest during a period with anthropogenic pollution (compare section 2 and Figure S1). The particles were internally mixed with carbonaceous (i.e., secondary organic material (SOM) and soot) and inorganic (i.e., ammoniated sulfate salts) constituents. We observed substantial morphological transformations with increasing RH and show that this microspectroscopic approach can provide new insights in the dynamic evolution of ambient aerosol particles under fluctuating atmospheric conditions.

2. Materials and Methods

Standard aerosols of NaCl, NaBr, and ammonium sulfate (AS, $(NH_4)_2SO_4$) were prepared by dissolving the pure compounds (Sigma Aldrich, St. Louis, MO, USA) in deionized water (Millipore–Milli Q plus 185, 18.2 MΩ cm) and spray-drying the aqueous solutions (0.1 M) using an atomizer (TSI Inc., Model 8026, St. Paul, MN, USA) combined with a silica-gel diffusion dryer. Aerosol samples were collected onto silicon nitride substrates (Si_3N_4, membrane width 500 μm, membrane thickness 100 nm, Silson Ltd, Northhampton, UK) using a single-stage impactor. Further sampling details are given in *Pöhlker et al.* [2012]. Samples were stored in airtight containers at 4°C and 20–30% RH.

Ambient aerosol samples were collected in the Amazonian rain forest at a remote site approximately 150 km northeast of Manaus, Brazil, during the transition period from dry to wet season (November–December 2012). The sampling site, Amazonian Tall Tower Observatory (ATTO, 2.14336°S, 59.0056°W, 120 m above sea level), is located in an untouched *terra firme* forest area that is characteristic for large parts of the Amazonian vegetation [*Junk and Piedade*, 2011]. During the wet season (December–May), the ATTO site is mostly under unpolluted air masses from the north-east, providing pristine atmospheric conditions. During the dry season (June–November), air masses from the south-east are frequently observed, carrying potential anthropogenic influence (i.e., biomass burning and urban emissions). The dry to wet transition period is characterized by an increasing frequency of precipitation and decreasing atmospheric concentrations of pyrogenic aerosols and trace gases from vegetation fires [*Andreae et al.*, 2012]. For the current study, back trajectories indicate light easterly winds with an influence from urbanized regions along the Amazon River (Figure S1). Here we focus on two representative samples (collected: 17 November and 24 November 2012) taken from a longer sampling period (17 November to 6 December 2012), which illustrate the characteristic composition and morphology of transition period particles and their transformations upon increasing RH.

Samples were collected below canopy through a stainless steel inlet and were dried with a silica diffusion dryer. The ambient RH during sampling was ~ 80%, the RH behind the diffusion dryer was ~ 40%, and the residence time of the particles in the dryer was 5 s. The ambient particles analyzed in this study are flattened on the substrate due to the impaction process, with an estimated relationship between the particle volume equivalent diameter D_{ve} and the diameter of the impacted particle D_{impact} of $D_{impact}/D_{ve} = ~ 3$ (section S1). Thus, the impacted particles analyzed here correspond to a size range of $D_{ve} = 0.1–1$ μm.
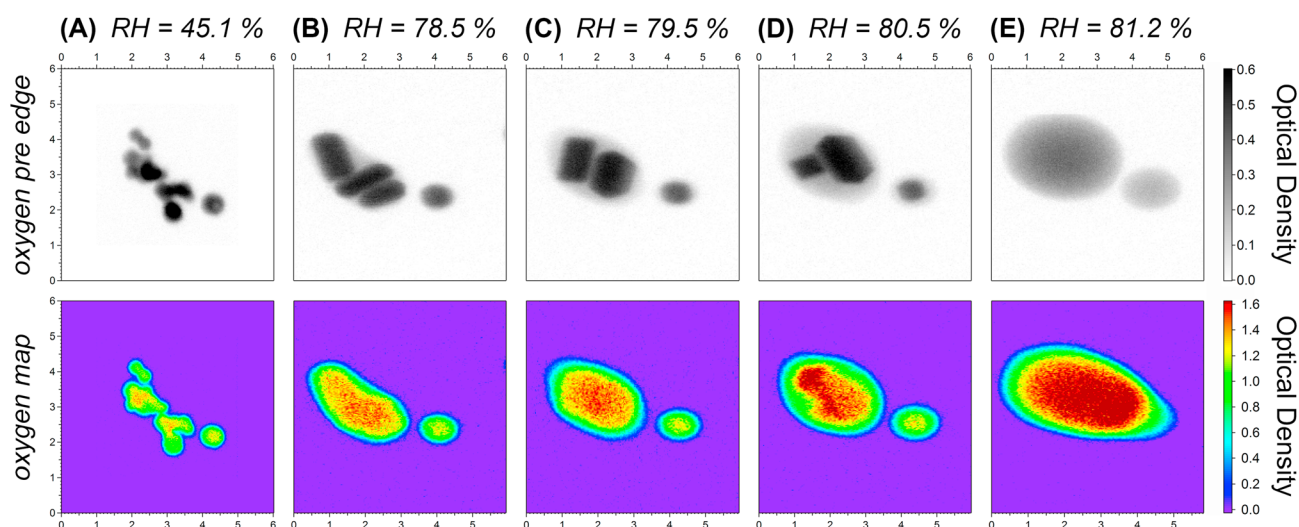
Figure 1. STXM images (grey) and oxygen elemental maps (colored) illustrating the hydration of ammonium sulfate standard particles at five selected RH levels. All images and maps show the same group of particles. (top row) Oxygen pre-edge images (at 528 eV) and (bottom row) oxygen elemental maps (pre-edge at 528 eV, postedge at 537 eV). (a–d) Particles show gradual water uptake with coexisting solid and liquid phases. Increasing water content raises ion mobility and provokes recrystallization of solid AS cores (Figures 1b–1d). (e) Deliquescence occurs at 80 ± 1%. X-ray absorption at the oxygen edge by water overwhelms absorption by sulfate, and therefore, the shape of ammonium sulfate cores can hardly be recognized in the oxygen maps in Figures 1b–1d. Axes display image dimensions in μm. Optical density (grey and color scales) is unified among Figure 1 (top row) images and among Figure 1 (bottom row) oxygen maps.

The STXM-NEXAFS analysis was conducted at the Magnetic X-ray Microscope with UHV Spectroscopy (MAXYMUS) beamline (UE46-PGM-2) at the synchrotron BESSY II, Helmholtz-Zentrum, Berlin, Germany. The MAXYMUS-STXM is equipped with a plane grating monochromator (600 lines mm^{-1} blazed) with a resolving power of $E/\Delta E \leq 8000$ at the carbon K-edge. A Fresnel zone plate provides a resolution of about 30 nm and a phosphor-coated Lucite tube with photomultiplier detects transmitted photons. Further instrument and data analysis related details can be found in *Follath et al.* [2010] and *Pöhlker et al.* [2012].

During the experiments, the RH was monitored by humidity and temperature sensors coupled to a data logger (model IP 60; MRS Electronics GmbH, Seuzach, Switzerland). The data logger was installed outside the STXM vacuum chamber, and the humidity and temperature sensors were connected through a vacuum flange. Both sensors were directly attached to the sample holder plate to ensure accurate humidity and temperature measurements close to the sample. The instrument chamber was first evacuated to < 0.1 hPa, and then the RH in the chamber was increased stepwise by opening a valve connected to a water container. After reaching the maximum RH, the RH was reduced again by pumping down the microscope chamber. During the RH cycle, the temperature at the sample remained constant at 27 ± 1°C. The RH increase and decrease rates in our experiment were $< 4\%$ min^{-1}. Cloud parcel modeling suggests that atmospheric RH fluctuations typically occur from 0 to 3.6% min^{-1} (H. Su, personal communication, 2013). We therefore assume that the water uptake in our experiments approximates atmospheric conditions and represents regimes without strong kinetic limitations [*Shiraiwa et al.*, 2013]. The accessible RH range from 0% to 86% is limited at the upper end by temperature gradients inside the instrument. Independently, the RH was calculated based on the chamber temperature and water partial pressure, confirming the measured RH results (Figure S2).

3. Results and Discussion

Aerosol particle standards of NaCl, NaBr, and AS were used for testing and calibration of the experimental setup, and the DRH of these compounds served as an independent check of the measured RH [*Ghorai and Tivanski*, 2010; *Zelenay et al.*, 2011]. Deliquescence of NaCl was observed at 77 ± 1% (literature: 75.3% [*Krieger et al.*, 2012]), NaBr at 50 ± 1% (47% [*Wise et al.*, 2005]), and AS at 81 ± 1% (literature: 80% [*Ebert et al.*, 2002]). In general, the experimental and literature DRH values correspond well, which confirms the reliability of the RH measurement. The slight deviation by about 2% could be explained by kinetic effects when the system had not reached full equilibrium. Prior to deliquescence, the substrate-supported AS particles showed substantial water uptake starting at 78%, forming an aqueous halo (up to 500 nm) around a solid AS core. This hydration was accompanied by a substantial transformation of the initial morphology (Figures 1a–1b).

Wise et al. [2008] have reported similar observations for NaCl hydration in environmental transmission electron microscopy. They hypothesize that this nonabrupt phase transition is in accordance with an extended version of the phase rule for substrate-supported particles and that the interactions at the sample/substrate interface play an important role as additional energy term, explaining the coexistence of solid and aqueous phase over a finite RH range. For airborne salt particles, a comparably significant water uptake prior to deliquescence has not been observed; however, the nonabrupt phase transition for salt standards on substrates may be relevant as a proxy for processes in mixed aerosol particles with soluble (e.g., AS and NaCl) and insoluble constituents (e.g., soot) [*Wise et al.*, 2008]. In the range of 78–80% RH, we observed diverse morphological transformations of the AS particles, such as the coexistence of solid and liquid phases, recrystallization of the solid salt cores resulting in the growth of larger crystals at the expense of smaller ones (Ostwald ripening), and a gradual shrinkage of the solid in favor of the liquid phase (Figures 1b–1d). Corresponding results for the NaCl and NaBr standards are displayed in Figures S3–S5.

Analogous to the hydration of standard aerosols, ambient aerosol samples from the Amazon rain forest were analyzed by X-ray microspectroscopy and examined for transformations as a function of RH. In this study, we focus on samples from the dry to wet season transition period, which consist of strongly internally mixed particles containing soot, SOM, and ammoniated sulfate salts as main constituents. The particle microstructure suggests strongly aged particles (Figure S6). It shows that soot "cores" are embedded in a mixture of sulfate salts and SOM, in which the inorganic constituents often occur as an "inner shell" and the SOM as an "outer shell." This "inner shell/outer shell morphology" could be explained by liquid-liquid phase separation (LLPS), as described in previous studies [*Bertram et al.*, 2011; *Song et al.*, 2012] (section S2). X-ray absorption spectra indicate that ammoniated sulfate and SOM are the main constituents of the internally mixed particles (Figures S7 and S8). The following dry particle composition was estimated: $O/C = 2.0 \pm 0.5$, $N/C = 0.9 \pm 0.2$, $N/O = 0.4 \pm 0.1$. The spectral shape at the nitrogen edge indicates ammonium as the dominant N species; however, the spectra do not allow a discrimination between AS $[(NH_4)_2SO_4]$, letovicite $[(NH_4)_3H(SO_4)_2]$, and ammonium bisulfate $[(NH_4)HSO_4]$ (section S3). Although potassium (K^+) has been found as a minor cation (in addition to NH_4^+), the K content in these anthropogenically influenced and strongly aged particles reported here is lower than previously observed in pristine rainy season aerosols [*Pöhlker et al.*, 2012]. The NEXAFS spectra at the carbon absorption edge reveal typical soot and SOM signatures (Figure S8).

Figure 2 displays oxygen elemental maps for a representative ensemble of particles and illustrates characteristic morphological transformations upon hydration across four RH levels. The dry aerosol particles (RH = 0%, Figure 2a) reveal a typical impaction morphology [*Freedman et al.*, 2010] with an estimated diameter-to-height ratio of ~ 10 (section S1). During sampling, the aerosol particles are dried out quickly, and the impacted material likely persists in an amorphous or polycrystalline (small crystallites embedded in organic matrix) state (no crystalline structure could be detected in these particles either by STXM or high-resolution SEM, e.g., Figure S11). Upon hydration, morphological changes were observed at 70% RH, where most of the impacted particles begin to reduce their diameter, presumably increasing their height, and form more compact structures with increased absorptivity. An explanation for this transformation can be the decreasing viscosity and increasing surface tension as a result of water uptake, which allows the particles to "bead up" by increasing their contact angle with the hydrophobic silicon nitride surface. This transformation continues with increasing RH levels (compare 80% RH in Figure 2c). At 87% RH, the particles reveal a droplet-like morphology with further elevated absorptivity at the oxygen edge, indicating partial and in some cases full deliquescence of the particles. X-ray absorption spectra confirm increasing optical densities at the oxygen K-edge with rising RH levels: prior to deliquescence, the water content is about 5 mol H_2O per mol SO_4^{2-}, whereas after deliquescence, a content of 13 mol H_2O per mol SO_4^{2-} is estimated (Figure S7). For comparison, 13 water molecules fit into the first solvation shell of sulfate in aqueous solution [*Cannon et al.*, 1994].

Figure 3 shows a close-up of a few selected particles and reveals the microstructural changes associated with the restructuring process. In the initial phase of this process, the inorganic material migrates into smaller and clearly defined structures that often show polygonal outlines, suggesting crystalline morphology. In contrast, the carbonaceous material (i.e., SOM and soot) on the impaction substrate remains mostly unchanged, apart from negative "footprints" of the inorganic components in the SOM. We suggest that (re)crystallization of the inorganic material in the internally mixed particles can explain the observed restructuring prior to deliquescence, based on the following observations: (i) Elemental ratios derived from X-ray absorption spectra and the characteristic spectral structure at the nitrogen and oxygen absorption edges underline that
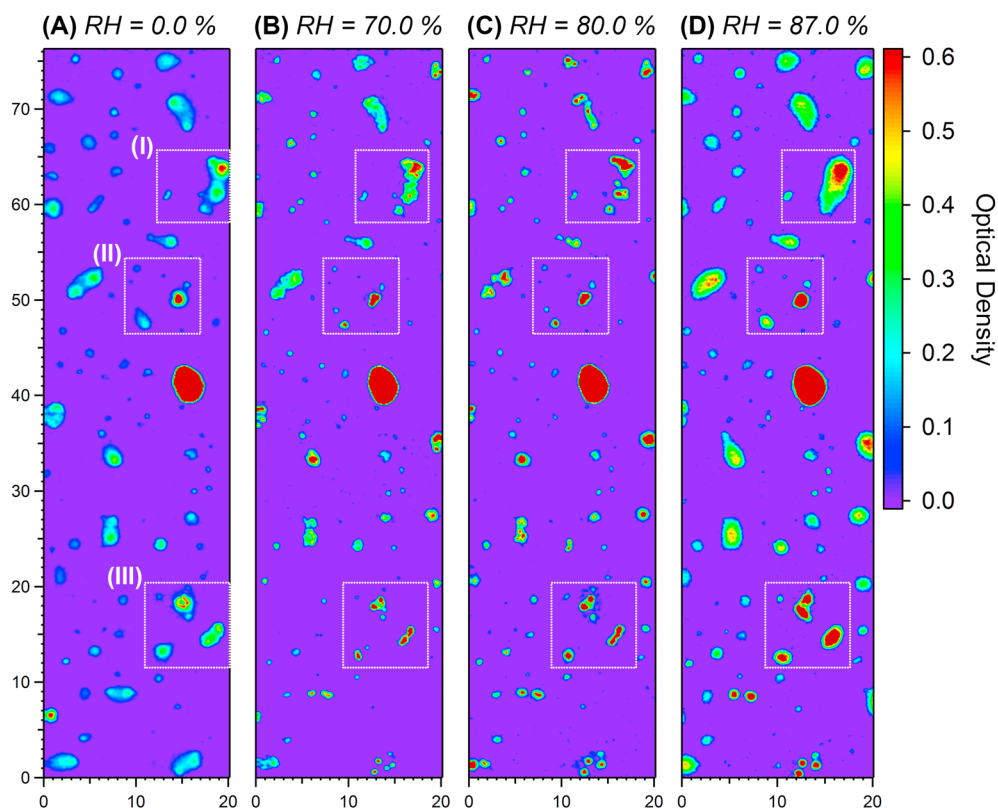
Figure 2. (a–d) STXM oxygen maps of a representative region in an Amazonian aerosol sample reveal substantial morphological transformations of aerosol particles with increasing RH. Restructuring of particles is observed at 70–80%. Oxygen map at 87% shows partially and fully deliquesced particles. Maps shown here represent the first hydration cycle of unaltered particles after sampling. Areas highlighted by white boxes represent the following: (I) close-up shown in Figure 4, (II) close-up shown in Figure S9, and (III) close-up shown in Figure 3. Axes display image dimensions in μm. Optical density (color code) is unified among all maps.

SO_4^{2-} and NH_4^+ are the dominant inorganic constituents. Therefore, the transformation of the ambient particles can be linked with the recrystallization of standard AS in Figure 1. (ii) The migration of certain elements into smaller and clearly defined structures is observed exclusively for the inorganic constituents (SO_4^{2-}, K^+, and NH_4^+) suggesting the formation of $(NH_4)_{2-x-y}H_xK_ySO_4$ (Figures 3 and S9). (iii) The structures formed reveal cubic crystal-like morphologies (Figures 3 and S9), which resemble the AS crystals displayed in Figure 1. LLPS, as an alternative explanation, would form droplet-like structures and therefore cannot explain the growth of crystal-like entities. The initially amorphous or microcrystalline state of the impacted particles is metastable toward an energetically favored increase in crystallization degree. Continuous water uptake by the particles with rising RH is accompanied by decreased viscosity and increased ion mobility and could overcome the kinetic inhibition of ion movement at a certain RH level. Potassium ions may facilitate the observed crystal formation, because of the lower solubility of K sulfates so that salts precipitating from an aqueous $K^+/NH_4^+/SO_4^{2-}$ solution are strongly enriched in K^+ compared to the solution K^+/NH_4^+ ratio [*Calvo and Simons*, 1952]. A further aspect is highlighted in Figures 3g–3h. Here overlay images of the carbon and oxygen elemental maps for low and high RH conditions are shown, illustrating that soot particles are initially embedded in an amorphous sulfate/SOM material. Upon hydration and crystallization of the ammoniated sulfate salts, the original microstructure changes and the soot is relocated to the particle's surface, instead of remaining in its center (Figure 3h). A restructuring of the particle and particularly the relocations of the soot cores in mixed aerosol particles can strongly change their optical and chemical properties (e.g., enhancement of absorption, affecting the reactive uptake of gas species) [*Bond et al.*, 2013; *Moffet and Prather*, 2009; *Schnaiter et al.*, 2005; *You et al.*, 2012]. In particular, a shift of the soot particles from the center of the particles to their surface would result in a pronounced decrease of the light absorption enhancement from internal mixing [*Adachi and Buseck*, 2013].
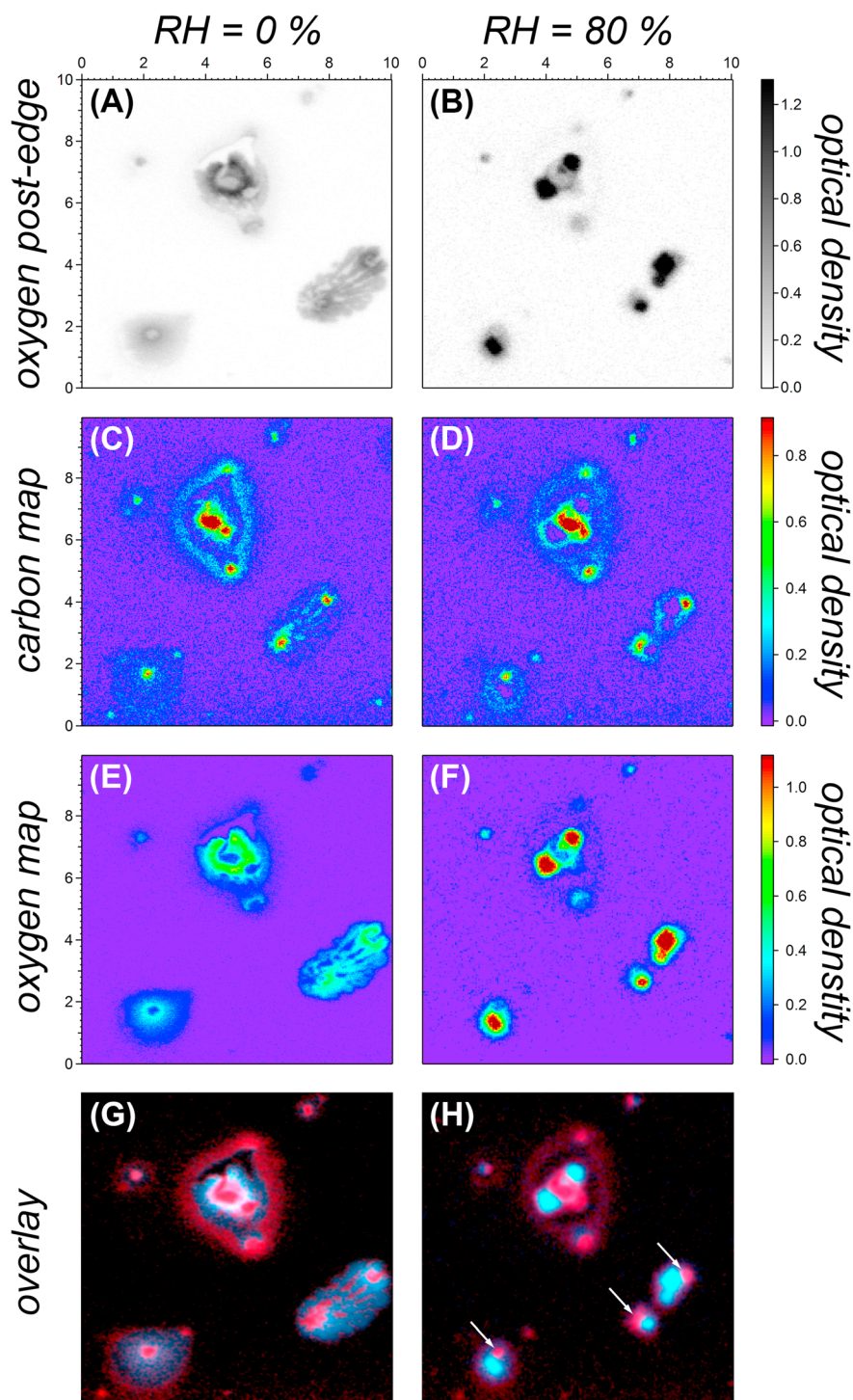
Figure 3. STXM images and elemental maps of representative internally mixed particles illustrating the microscale transformations of inorganic constituents with increasing RH. (a and b) Oxygen postedge images, (c and d) carbon elemental maps, (e and f) oxygen maps, and (g and h) overlay of carbon and oxygen map (C = red, O = blue). Images and maps in Figures 3a, 3c, 3e, and 3g are recorded at RH = 0% and in Figures 3b, 3d, 3f, and 3h at RH = 80%. Cubic structures in Figures 3b and 3f suggest that sulfate salts crystallize upon humidification. Highly absorbing spots in carbon maps represent soot particles (see Figure S6). At 0% RH, soot is incorporated in amorphous inorganic material (i.e., AS), while at 80% RH soot is localized on the surface of inorganic crystals (white arrows in Figure 3f). Axes in Figures 3a–3f display image dimensions in μm. Optical density (color code) is unified among Figures 3a and 3b, 3c and 3d, and 3e and 3f. Further STXM maps for potassium, pi, and sulfur of same area can be found in Figure S10.
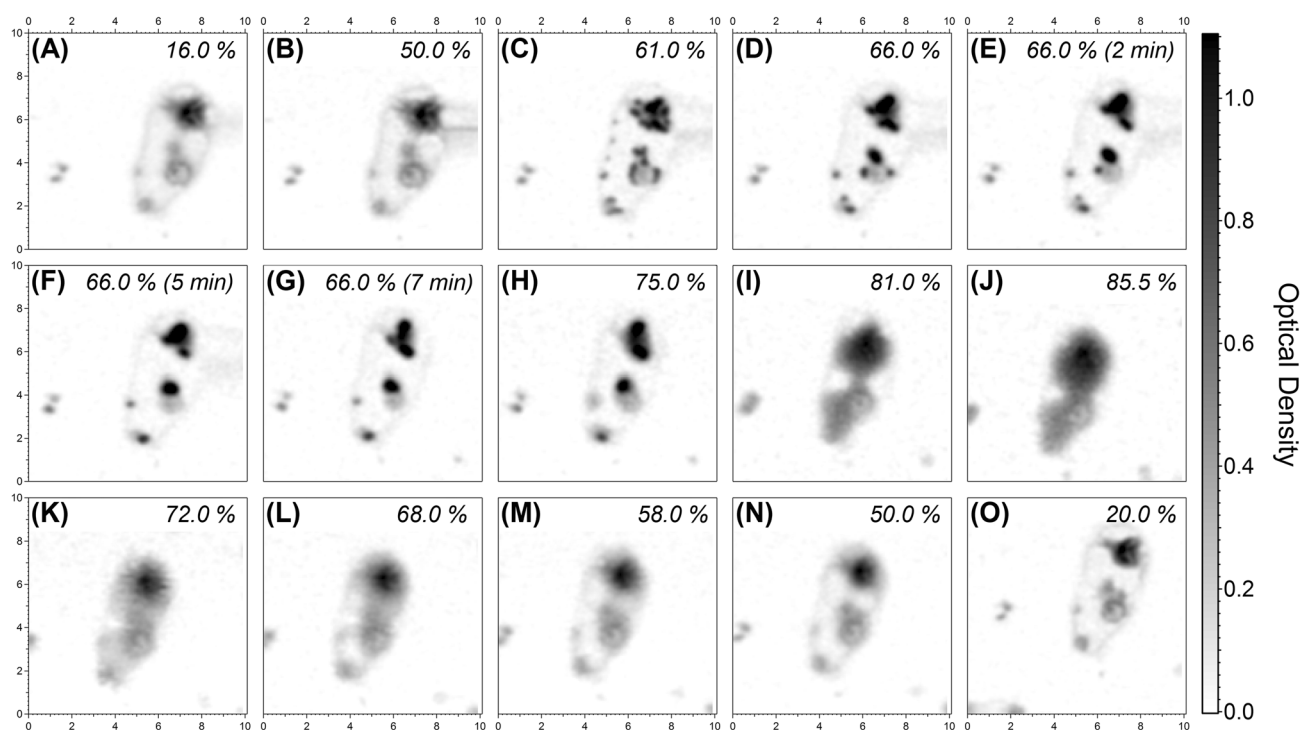
Figure 4. Sequence of oxygen postedge images (337 eV) illustrating the restructuring process of sulfate salts in internally mixed ambient particles during hydration and dehydration cycles. STXM images here represent second hydration cycle after first cycle, shown in Figures 2 and 3. An early state of ammoniated sulfate crystallization (formation of small nuclei-like structures) is observed (c) at 61%, (d–h) followed by restructuring with increasing RH and progressing time. Upon increasing RH, recrystallization causes growth of larger salt particles and shrinkage of smaller ones due to Ostwald ripening. Deliquescence occurs between 75 and 80%. Upon dehydration, particle water content decreases and (o) the remaining particle residues resemble (a) the initial state. Axes display image dimensions in μm. Optical density (grey scale) is unified among all images.

Figure 4 displays a series of STXM image scans on one selected particle from Figure 2. It illustrates morphology and phase transitions on the basis of smaller RH increments, showing that morphological transformations start at 60% RH with the formation of many small inorganic nuclei-like structures. Based on the previous observations, we assume that Figure 4c displays an early state of crystal growth in the course of either nucleation from an amorphous state or upon Ostwald ripening starting from a microcrystalline material. With increasing RH and ion mobility, the small crystals shrink and disappear in favor of larger ones that keep growing. At 75% RH, many small crystals have been converted to few larger ones. Above 80%, RH deliquescence occurs and strong water uptake is observed. This DRH of the mixed $(NH_4)_{2-x-y}H_xK_ySO_4$/SOM particles (O:C of SOM = 0.6 ± 0.2; SOM:SO_4^{2-} mass ratio = 0.4 ± 0.1) is in agreement with the predictions by *Bertram et al.* [2011]. The morphological appearance of the particle residue before (Figure 4b) and after (Figure 4o) the full hydration and dehydration cycle appears similar. Moreover, the restructuring is reproducible in subsequent hydration cycles. Here Figure 2 shows the first hydration cycle of the unaltered particles after sampling, whereas Figure 4 represents the second cycle on the same sample.

4. Summary and Atmospheric Implications

Water has a crucial influence on the physical and chemical properties of aerosol particles in the atmosphere. X-ray microspectroscopy under variable RH conditions is a suitable technique for in situ monitoring of aerosol hydration cycles on single particle basis. This technique has been applied to ambient aerosol samples for the first time and initial results are presented here. Aerosol samples were collected in the Amazonian rain forest during the transition period from dry to wet season and comprise strongly internally mixed particles with ammoniated sulfate, SOM, and soot as the main constituents. This aerosol particle type is characteristic for many locations with substantial anthropogenic influence worldwide and plays an important role in atmospheric cycling and climate (e.g., light absorption and cloud formation) [*Adachi and Buseck*, 2008; *Bond et al.*, 2013; *Colberg et al.*, 2004; *Posfai et al.*, 1999]. The microstructure of these globally abundant

$(NH_4)_{2-x-y}H_xK_ySO_4$/SOM/soot particles is presented here, and our results provide further insights into their composition and mixing state and, thus, are potentially relevant for aerosol cycling in other locations worldwide.

Upon hydration we found substantial and reproducible morphological transformations in the range of 60–80% RH prior to particle deliquescence, with the apparently paradoxical phenomenon of efflorescence during hydration. An explanation for this observation can be the crystallization of formerly amorphous and/or microcrystalline sulfate salts in the particles. We suggest that the restructurings reported here are also relevant under atmospheric conditions. The hydration and drying rates in the microscopy setup were chosen to approximate corresponding rates in the atmosphere. Further, the experimental RH span where morphological changes were found (60–80%) corresponds to typical atmospheric conditions in the Amazon, where similar strong RH fluctuations prevail during vertical convection and in the course of the diurnal cycle. Given that similar processes occur in the atmosphere, important implications for aerosol cycling have to be considered. One such aspect is the relocation of soot cores in internally mixed particles from their center to the surface, as observed upon hydration. Such differences in mixing state can strongly alter the overall optical absorptivity of aerosol particles [*Bond et al.*, 2013]. A more detailed and quantitative analysis has to be addressed in further studies.

References

Adachi, K., and P. R. Buseck (2008), Internally mixed soot, sulfates, and organic matter in aerosol particles from Mexico City, *Atmos. Chem. Phys.*, *8*(21), 6469–6481, doi:10.5194/acp-8-6469-2008.

Adachi, K., and P. R. Buseck (2013), Changes of ns-soot mixing states and shapes in an urban area during CalNex, *J. Geophys. Res. Atmos.*, *118*, 3723–3730, doi:10.1002/jgrd.50321.

Adachi, K., E. J. Freney, and P. R. Buseck (2011), Shapes of internally mixed hygroscopic aerosol particles after deliquescence, and their effect on light scattering, *Geophys. Res. Lett.*, *38*, L13804, doi:10.1029/2011GL047540.

Andreae, M. O., and D. Rosenfeld (2008), Aerosol-cloud-precipitation interactions. Part 1. The nature and sources of cloud-active aerosols, *Earth Sci. Rev.*, *89*(1–2), 13–41, doi:10.1016/j.earscirev.2008.03.001.

Andreae, M. O., P. Artaxo, V. Beck, M. Bela, S. Freitas, C. Gerbig, K. Longo, J. W. Munger, K. T. Wiedemann, and S. C. Wofsy (2012), Carbon monoxide and related trace gases and aerosols over the Amazon Basin during the wet and dry seasons, *Atmos. Chem. Phys.*, *12*(13), 6041–6065, doi:10.5194/acp-12-6041-2012.

Bertram, A. K., S. T. Martin, S. J. Hanna, M. L. Smith, A. Bodsworth, Q. Chen, M. Kuwata, A. Liu, Y. You, and S. R. Zorn (2011), Predicting the relative humidities of liquid-liquid phase separation, efflorescence, and deliquescence of mixed particles of ammonium sulfate, organic material, and water using the organic-to-sulfate mass ratio of the particle and the oxygen-to-carbon elemental ratio of the organic component, *Atmos. Chem. Phys.*, *11*(21), 10,995–11,006.

Bond, T. C., et al. (2013), Bounding the role of black carbon in the climate system: A scientific assessment, *J. Geophys. Res. Atmos.*, *118*, 2169–8996, doi:10.1002/jgrd.50171.

Calvo, C., and E. L. Simons (1952), The ternary aqueous systems of ammonium sulfate with cesium, potassium and rubidium sulfates, *J. Am. Chem. Soc.*, *74*(5), 1202–1203.

Cannon, W. R., B. M. Pettitt, and J. A. McCammon (1994), Sulfate anion in water: Model structural, thermodynamic, and dynamic properties, *J. Phys. Chem.*, *98*(24), 6225–6230, doi:10.1021/j100075a027.

Colberg, C. A., U. K. Krieger, and T. Peter (2004), Morphological investigations of single levitated $H_2SO_4/NH_3/H_2O$ aerosol particles during deliquescence/efflorescence experiments, *J. Phys. Chem. A*, *108*(14), 2700–2709.

Ebert, M., M. Inerle-Hof, and S. Weinbruch (2002), Environmental scanning electron microscopy as a new technique to determine the hygroscopic behaviour of individual aerosol particles, *Atmos. Environ.*, *36*(39–40), 5909–5916, doi:10.1016/s1352-2310(02)00774-4.

Follath, R., J. S. Schmidt, M. Weigand, and K. Fauth (2010), The X-ray microscopy beamline UE46-PGM2 at BESSY, in *Sri 2009: The 10th International Conference on Synchrotron Radiation Instrumentation*, vol. 1234, edited by R. Garrett et al., pp. 323–326, American Institute of Physics, Melville, N. Y., doi:10.1063/1.3463201.

Freedman, M. A., K. J. Baustian, M. E. Wise, and M. A. Tolbert (2010), Characterizing the morphology of organic aerosols at ambient temperature and pressure, *Anal. Chem.*, *82*(19), 7965–7972, doi:10.1021/ac101437w.

Freney, E. J., K. Adachi, and P. R. Buseck (2010), Internally mixed atmospheric aerosol particles: Hygroscopic growth and light scattering, *J. Geophys. Res.*, *115*, D19210, doi:10.1029/2009JD013558.

Ghorai, S., and A. V. Tivanski (2010), Hygroscopic behavior of individual submicrometer particles studied by X-ray spectromicroscopy, *Anal. Chem.*, *82*(22), 9289–9298, doi:10.1021/ac101797k.

Jacobson, M. Z. (2001), Strong radiative heating due to the mixing state of black carbon in atmospheric aerosols, *Nature*, *409*(6821), 695–697, doi:10.1038/35055518.

Junk, W., and M. F. Piedade (2011), An introduction to South American wetland forests: Distribution, definitions and general characterization, in *Amazonian Floodplain Forests*, edited by W. J. Junk et al., pp. 3–25, Springer, Netherlands, doi:10.1007/978-90-481-8725-6_1.

Koop, T., J. Bookhold, M. Shiraiwa, and U. Pöschl (2011), Glass transition and phase state of organic compounds: Dependency on molecular properties and implications for secondary organic aerosols in the atmosphere, *Phys. Chem. Chem. Phys.*, *13*(43), 19,238–19,255, doi:10.1039/c1cp22617g.

Krieger, U. K., C. Marcolli, and J. P. Reid (2012), Exploring the complexity of aerosol particle properties and processes using single particle techniques, *Chem. Soc. Rev.*, *41*(19), 6631–6662, doi:10.1039/c2cs35082c.

Lee, S. H., D. M. Murphy, D. S. Thomson, and A. M. Middlebrook (2002), Chemical components of single particles measured with Particle Analysis by Laser Mass Spectrometry (PALMS) during the Atlanta SuperSite Project: Focus on organic/sulfate, lead, soot, and mineral particles, *J. Geophys. Res.*, *107*(D1), 4003, doi:10.1029/2000JD000011.

Martin, S. T. (2000), Phase transitions of aqueous atmospheric particles, *Chem. Rev.*, *100*(9), 3403–3453, doi:10.1021/cr990034t.

Mikhailov, E., S. Vlasenko, S. T. Martin, T. Koop, and U. Pöschl (2009), Amorphous and crystalline aerosol particles interacting with water vapor: Conceptual framework and experimental evidence for restructuring, phase transitions and kinetic limitations, *Atmos. Chem. Phys.*, *9*(24), 9491–9522, doi:10.5194/acp-9-9491-2009.

Moffet, R. C., and K. A. Prather (2009), In-situ measurements of the mixing state and optical properties of soot with implications for radiative forcing estimates, *Proc. Natl. Acad. Sci. U. S. A.*, *106*(29), 11,872–11,877, doi:10.1073/pnas.0900040106.

Moffet, R. C., H. Furutani, T. C. Roedel, T. R. Henn, P. O. Sprau, A. Laskin, M. Uematsu, and M. K. Gilles (2012), Iron speciation and mixing in single aerosol particles from the Asian continental outflow, *J. Geophys. Res.*, *117*, D07204, doi:10.1029/2011JD016746.

Peckhaus, A., S. Grass, L. Treuel, and R. Zellner (2012), Deliquescence and efflorescence behavior of ternary inorganic/organic/water aerosol particles, *J. Phys. Chem. A*, *116*(24), 6199–6210, doi:10.1021/jp211522t.

Pöhlker, C., et al. (2012), Biogenic potassium salt particles as seeds for secondary organic aerosol in the Amazon, *Science*, *337*(6098), 1075–1078, doi:10.1126/science.1223264.

Posfai, M., J. R. Anderson, P. R. Buseck, and H. Sievering (1999), Soot and sulfate aerosol particles in the remote marine troposphere, *J. Geophys. Res.*, *104*(D17), 21,685–21,693, doi:10.1029/1999JD900208.

Ramanathan, V., P. J. Crutzen, J. T. Kiehl, and D. Rosenfeld (2001), Aerosols, climate, and the hydrological cycle, *Science*, *294*(5549), 2119–2124, doi:10.1126/science.1064034.

Rosenfeld, D., U. Lohmann, G. B. Raga, C. D. O'Dowd, M. Kulmala, S. Fuzzi, A. Reissell, and M. O. Andreae (2008), Flood or drought: How do aerosols affect precipitation?, *Science*, *321*(5894), 1309–1313, doi:10.1126/science.1160606.

Russell, L. M., S. F. Maria, and S. C. B. Myneni (2002), Mapping organic coatings on atmospheric particles, *Geophys. Res. Lett.*, *29*(16), 1779, doi:10.1029/2002GL014874.

Schnaiter, M., C. Linke, O. Mohler, K. H. Naumann, H. Saathoff, R. Wagner, U. Schurath, and B. Wehner (2005), Absorption amplification of black carbon internally mixed with secondary organic aerosol, *J. Geophys. Res.*, *110*, D19204, doi:10.1029/2005JD006046.

Shiraiwa, M., A. Zuend, A. K. Bertram, and J. H. Seinfeld (2013), Gas-particle partitioning of atmospheric aerosols: Interplay of physical state, non-ideal mixing and morphology, *Phys. Chem. Chem. Phys.*, *15*(27), 11,441–11,453, doi:10.1039/C3CP51595H.

Solomon, S., D. Qin, Z. Manning, Z. Chen, M. Marquis, K. B. Avery, M. Tignor, and H. L. E. Miller (2007), IPCC 4th assessment report, Cambridge Univ. Press, Cambridge, U. K.

Song, M., C. Marcolli, U. K. Krieger, A. Zuend, and T. Peter (2012), Liquid-liquid phase separation and morphology of internally mixed dicarboxylic acids/ammonium sulfate/water particles, *Atmos. Chem. Phys.*, *12*(5), 2691–2712, doi:10.5194/acp-12-2691-2012.

ten Brink, H. M., A. Khlystov, G. P. A. Kos, T. Tuch, C. Roth, and W. Kreyling (2000), A high-flow humidograph for testing the water uptake by ambient aerosol, *Atmos. Environ.*, *34*(25), 4291–4300, doi:10.1016/s1352-2310(00)00197-7.

Tivanski, A. V., R. J. Hopkins, T. Tyliszczak, and M. K. Gilles (2007), Oxygenated interface on biomass burn tar balls determined by single particle scanning transmission X-ray microscopy, *J. Phys. Chem. A*, *111*(25), 5448–5458, doi:10.1021/jp070155u.

Wang, J., D. J. Jacob, and S. T. Martin (2008), Sensitivity of sulfate direct climate forcing to the hysteresis of particle phase transitions, *J. Geophys. Res.*, *113*, D11207, doi:10.1029/2007JD009368.

Wise, M. E., S. T. Martin, L. M. Russell, and P. R. Buseck (2008), Water uptake by NaCl particles prior to deliquescence and the phase rule, *Aerosol Sci. Technol.*, *42*(4), 281–294.

Wise, M. E., G. Biskos, S. T. Martin, L. M. Russell, and P. R. Buseck (2005), Phase transitions of single salt particles studied using a transmission electron microscope with an environmental cell, *Aerosol Sci. Technol.*, *39*(9), 849–856, doi:10.1080/02786820802047115.

You, Y., et al. (2012), Images reveal that atmospheric particles can undergo liquid-liquid phase separations, *Proc. Natl. Acad. Sci. U.S.A.*, *109*(33), 13,188–13,193, doi:10.1073/pnas.1206414109.

Zelenay, V., M. Ammann, A. Krepelova, M. Birrer, G. Tzvetkov, M. G. C. Vernooij, J. Raabe, and T. Huthwelker (2011), Direct observation of water uptake and release in individual submicrometer sized ammonium sulfate and ammonium sulfate/adipic acid particles using X-ray microspectroscopy, *J. Aerosol Sci.*, *42*(1), 38–51, doi:10.1016/j.jaerosci.2010.11.001.